Journal of Fluids and Structures (2000) **14,** 993–1011
doi:10.1006/jfls.2000.0307, available online at http://www.idealibrary.com on IDEAL®

EFFECTS OF A TRANSLATING LOAD ON A FLOATING PLATE—STRUCTURAL DRAG AND PLATE DEFORMATION†

R. W. YEUNG

Mechanical Engineering and Ocean Engineering, University of California at Berkeley
Berkeley, CA 94720-1740, U.S.A.
and
Institut für Schiffstechnik, Mercator University of Duisburg
D-47048, Duisburg, Germany.

AND

J. W. KIM

Department of Ocean and Resources Engineering, University of Hawaii at Manoa
Honolulu, HI 96822-2303, U.S.A.

(Received 8 March 1999, and in final form 3 May 2000)

The elastic deformation of a structural plate floating on water caused by a translating three-dimensional load is investigated. The problem is akin to the landing and take-off of aircraft on a structural or ice sheet. The initial-boundary-value problem is solved analytically using a free-surface condition that incorporates the flexural rigidity of the plate. The three-dimensional load is modeled as an axisymmetric, translating pressure distribution. The time-dependent analytical solution is used to obtain the unsteady drag of this moving pressure, if it exists, as well as its asymptotic behavior at large time. The behavior of the transition of the drag near a critical speed related to the minimum celerity of the free waves of the hydroelastic system is examined. Asymptotic analysis shows that the drag attains a discontinuous but finite value as the translation speed approaches the critical speed, an essential difference from some existing two-dimensional results. The growth rate of the plate slope is found to be weakly singular, like $\log t$, for large time. Comparisons with published experimental data for plate deformation are made for the case of an ice sheet. The agreement is very favorable. Implications on the operation of floating runways are discussed.

1. INTRODUCTION

MAT-TYPE STRUCTURES are considered to be one of the most promising designs for floating airports or runways, particularly in more sheltered areas. Their relatively simple construction and ease of maintenance offer distinct advantages. The MegaFloat prototype project in Japan [see e.g. Watanabe (1996)] is an excellent illustration of this concept. The structure could be as long as 4 km, as wide as 1 km, but has a draft of only a few meters. These proportions render the structure to be mat- or sheet-like, which will respond flexurally under wave excitations, or even under moving loads such as those imparted by an aircraft during landing or take-off. Since the wave-induced motion and deflection can easily impose

† Preliminary paper presented at the 2nd International Conference on Hydroelasticity in Marine Technology, Fukuoka, Japan, December 1998.

0889–9746/00/100993 + 19 $35.00/0

operational limits on the runway, the response of such a structure to incoming waves has been a subject of many studies [e.g. Ertekin *et al.* (1994), Mamidipudi & Webster (1994), Newman *et al.* (1996), Kashiwagi (1996), Ertekin & Kim (1999)].

A related issue is the response of the runway to the moving load itself. The flexural rigidity is typically such that structural waves will be generated, thus inducing additional drag and undulations that may interfere with the safe operation of an aircraft. Deformation of such a mat-like floating structure is akin to the problem of aircraft landing on ice sheets in Arctic and Antarctic regions. Motivated by an interest in polar expeditions, several major theoretical and experimental studies have been undertaken to understand the effect of aircraft and vehicle operation on floating ice (Davys *et al.* 1985; Schulkes & Sneyd 1988; Milinazzo *et al.* 1995). When modeled as a continuous, flexural material, the ice sheet is found to exhibit structural deflections which may impede the operation of these natural runways. The deflection leads to a critical speed of this structure–fluid system. If the moving load operates near this speed, according to Kheshin (1963) and Nevel (1970), a steady-state solution may not exist. This critical speed was identified by Kerr (1983) as one associated with the minimum celerity $C_{\min}$ of the structure–fluid wave system. In fact, Davys *et al.* (1985) argued that the phenomenon was due to an accumulation of the energy near the load since the group velocity and the celerity have the same value at the critical speed.

The present study is motivated by a concern that the same resonant phenomenon may cause difficulties on floating runways. Although the artificial floating runway is stiffer than ice sheets, the loads applied to the runway are much larger than those on the ice sheet and the phenomenon of critical speed should not be ignored without a careful study. The asymptotic results of Schulkes & Sneyd (1988) in two dimensions suggest that the growth of the surface slope around the loading, thus possibly also the drag on the plate, is unbounded. This conclusion may need to be suitably modified in the presence of three-dimensional effects since energy can radiate in lateral directions.

In this study, we formulate the time-dependent three-dimensional problem that describes the deformation of a thin elastic plate floating on water, with excitation caused by a translating axisymmetric pressure. After some order-of-magnitude arguments and numerical verification, the model is shown to simplify to a point load translating on a massless, elastic plate. These reductions are due to the fact that the wavelength of the free waves, which cause the resonant phenomenon, is much greater than the length scale of the loading and sheet thickness. With this simplification, all the nondimensional physical variables can be represented as functions of a single parameter, $U_D = U/C_{\min}$, where U is the translation speed of the load. By sacrificing some details of the problem, we obtain explicit formulas for speed, wavelength, steady drag, and maximum deflection at the critical speed, which can be used to estimate the performance of floating runways at this resonant condition.

The solution of the unsteady-flow problem is obtained following the procedure of Yeung (1975), who considered arbitrary planar motion of a pressure distribution on the water surface. The floating elastic plate is modeled in the same manner as Davys *et al.* (1985). An explicit solution for the load translating with uniform speed after finite period of acceleration is derived. The solution can be decomposed into three parts, representing the contributions from the initial deflection, initial acceleration, and uniform-speed translation. However, further analysis is made only on the uniform-translation part since our primary goal is to study the resonant phenomenon due to translation at critical speed. Asymptotic analysis is made for the time-dependent solution to obtain steady and asymptotic behavior of drag and deflection at large time. The asymptotic result shows that the time rate of growth of the deflection at the critical speed is weaker than that in two dimensions and the loading achieves a steady drag for all speeds. Some testing of this theory is made by comparisons with certain existing measurements from ice sheets.

2. FORMULATION OF THE PROBLEM

Consider an infinite isotropic elastic plate of mass m (per unit area) floating on an infinitely deep, inviscid, fluid of density ρ, as shown in Figure 1. A Cartesian coordinate system $Oxyz$ is defined here with the z-axis directed vertically upward and the Oxy plane being the still interface between the water and the plate. We will investigate the deflection of the plate caused by an axisymmetric moving load translating along the x-axis with velocity $X(t)$,

$$p = p(\bar{r}) = p(\sqrt{\bar{x}^2 + y^2}). \tag{1}$$

Here, $\bar{x} \equiv x - X(t)$ and $\bar{r} \equiv \sqrt{\bar{x}^2 + y^2}$ are introduced to define a moving Cartesian coordinate system $\bar{O}\bar{x}yz$ and a polar coordinate system $\bar{O}\bar{r}\bar{\theta}$ where the origin is fixed to the center of the loading. The motion of the load is given differently in two phases of motion as shown in Figure 2:

$$\dot{X}(t) = \begin{cases} Ut/t_s, & t < t_s \\ U, & t > t_s \end{cases}, \qquad X(t) = \begin{cases} (U/2t_s)t^2, & t < t_s \\ U(t - t_s) + \frac{1}{2}Ut_s, & t > t_s. \end{cases} \tag{2}$$

The load translates with a constant speed, U, after accelerating during the period $0 < t < t_s$ with uniform acceleration U/t_s.

The loading function $p(\bar{r})$ is parametrically represented as

$$p(\bar{r}) = \frac{P}{R} f\left(\frac{\bar{r}}{R}\right) \tag{3}$$

using the magnitude of the loading P (e.g. total weight of load) and an effective radius of the loading R. The function f determines the shape of the loading and is normalized as

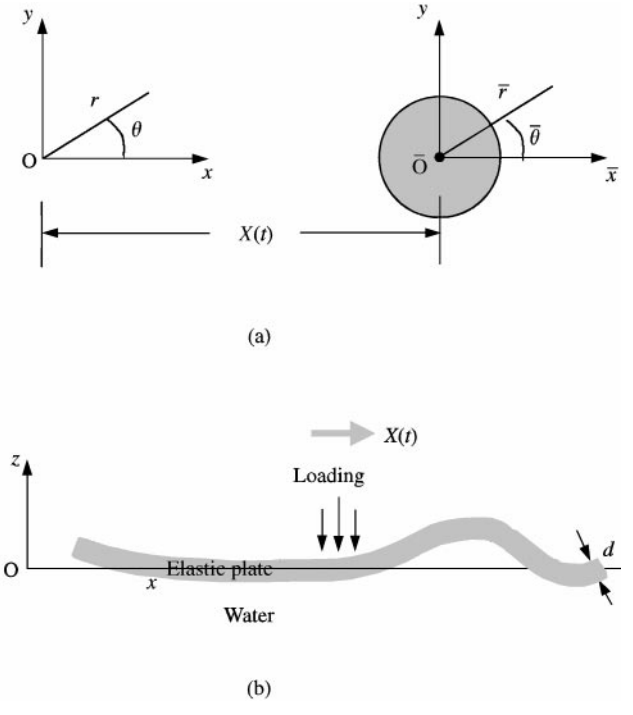

Figure 1. Coordinate system: (a) plan view; (b) elevation.

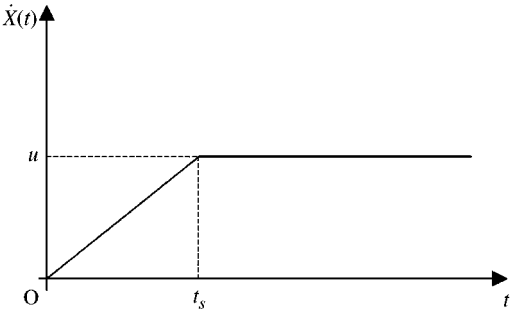

Figure 2. Time history of velocity of pressure loading.

$2\pi\int_0^\infty f(\bar{r})\bar{r}\,\mathrm{d}\bar{r} = 1$. For an example, we can take f as a Gaussian distribution,

$$f(\bar{r}) = \mathrm{e}^{-\pi\bar{r}^2}, \tag{4}$$

which was also used in two-dimensional analysis of Kim & Webster (1998). In this case, the effective radius R is defined such that 95% of the loading is confined in the region $\bar{r} < R$.

We assume that the draft of the plate, d, is sufficiently smaller than the length of the waves caused by the moving load, so that we can use thin-plate theory to describe the vertical deflection of the plate, $w(x, y, t)$. The equation of motion of the plate is given by the thin-plate equation [see, e.g., Davys *et al.* (1985)]:

$$mw_{tt} + D\Delta^2 w + \rho g w = -\rho\phi_t|_{z=0} - p, \tag{5}$$

where $\Delta \equiv \partial^2/\partial x^2 + \partial^2/\partial y^2$ is the Laplacian operator defined on the horizontal plane and $D = EI/(1-\nu^2)$ (E being Young's modulus, I the moment of inertia of the plate section per unit width, ν the Poisson ratio) is the flexural rigidity of the plate; $\phi(x, y, z, t)$ is the velocity potential of the irrotational flow under the plate. We assume further that the load starts from the rest. Then the initial condition can be given as

$$w(x, y, 0) = w_0(x, y), \qquad w_t(x, y, 0) = 0, \tag{6}$$

where the initial deflection w_0 can by obtained by solving the static equation

$$D\Delta^2 w_0 + \rho g w_0 = -p. \tag{7}$$

The velocity potential $\phi(x, y, z, t)$ should satisfy the Laplace equation in the fluid domain with no-leak conditions under the plate surface:

$$\nabla^2\phi = 0, \qquad z < 0, \tag{8}$$

$$\phi_z = w_t, \qquad z = 0, \tag{9}$$

$$|\nabla\phi| \to 0, \qquad z \to -\infty. \tag{10}$$

3. SOLUTION BY FOURIER TRANSFORMS

It is common to obtain solution of the formulated problem in Section 2 by Fourier transforms [see, e.g. Yeung (1975), Schulkes & Sneyd (1988)] since all boundary conditions are applied on planar surfaces. As a solution procedure for the equations of motion given in

the previous section, we adopt the method of Fourier transformation following Schulkes & Sneyd (1988). Taking the Fourier transforms of equations (5), (8) and (9), we obtain

$$m\tilde{w}_{tt} + (Dk^4 + \rho g)\tilde{w} = -\rho\tilde{\phi}_t|_{z=0} - \tilde{p}\exp[(ik\cos\alpha)\,X(t)], \tag{11}$$

$$\tilde{\phi}_{zz} - k^2\tilde{\phi} = 0, \quad z < 0, \tag{12}$$

$$\tilde{\phi}_z = \tilde{w}_t, \quad z = 0, \tag{13}$$

respectively. Note that in this frame of reference, the speed of the load p is implicitly contained in $X(t)$. Here, the transformed variables $\tilde{w}$, $\tilde{\phi}$ and $\tilde{p}$ are defined as

$$\tilde{w}(k, \alpha, t) = \int_0^\infty \int_0^{2\pi} w(r\cos\theta, r\sin\theta, t)\,\mathrm{e}^{\mathrm{i}kr\cos(\alpha-\theta)}\,r\,\mathrm{d}\theta\,\mathrm{d}r,$$

$$\tilde{\phi}(k, \alpha, z, t) = \int_0^\infty \int_0^{2\pi} \phi(r\cos\theta, r\sin\theta, z, t)\,\mathrm{e}^{\mathrm{i}kr\cos(\alpha-\theta)}\,r\,\mathrm{d}\theta\,\mathrm{d}r,$$

$$\tilde{p}(k) = \int_{-\infty}^\infty \int_0^{2\pi} p(r)\,\mathrm{e}^{\mathrm{i}kr\cos(\alpha-\theta)}\,r\,\mathrm{d}\theta\,\mathrm{d}r = 2\pi\int_0^\infty rp(r)\,\mathrm{J}_0(kr)\,\mathrm{d}r, \tag{14}$$

where we have adopted cylindrical coordinates (r, θ, z) in the physical space and (k, α, z) in the transformed space; J_0 is the Bessel function of order zero.

From equations (12) and (13) we can obtain

$$\tilde{\phi} = \frac{\tilde{w}_t}{k}\,\mathrm{e}^{kz}. \tag{15}$$

A substitution of equation (15) into equation (11) yields the equation of motion of the plate in the transformed space:

$$M(k)\tilde{w}_{tt} + K(k)\tilde{w} = -\tilde{p}(k)\exp[(\mathrm{i}k\cos\alpha)\,X(t)], \tag{16}$$

where

$$M(k) \equiv m + \frac{\rho}{k}, \quad K(k) \equiv Dk^4 + \rho g. \tag{17}$$

The solution of equation (16) is given by

$$\tilde{w} = -\frac{\tilde{p}(k)}{M(k)\omega(k)}\int_0^t \sin\omega(t-\tau)\,\mathrm{e}^{\mathrm{i}k\cos\alpha X(\tau)}\,\mathrm{d}\tau + \tilde{w}_0(k)\cos\omega t, \tag{18}$$

where

$$\omega(k) = \sqrt{\frac{K}{M}} = k\sqrt{\frac{Dk^4 + \rho g}{mk^2 + \rho k}}, \tag{19}$$

and $\tilde{w}_0(k)$ can be obtained from the static solution of equation (16) as

$$\tilde{w}_0(k) = -\frac{\tilde{p}(k)}{K(k)} = -\frac{\tilde{p}}{Dk^4 + \rho g}. \tag{20}$$

Taking the inverse Fourier transform, we obtain

$$w = -\frac{1}{4\pi^2}\int_0^\infty \frac{k\tilde{p}}{M\omega}\int_0^t \sin[\omega(t-\tau)]\int_0^{2\pi} e^{ik[(x-X(\tau))\cos\alpha + y\sin\alpha]}\,d\alpha\,d\tau\,dk$$
$$+\frac{1}{4\pi^2}\int_0^\infty k\tilde{w}_0\cos\omega t\int_0^{2\pi} e^{ikr\cos(\theta-\alpha)}\,d\alpha\,dk$$
$$= -\frac{1}{2\pi}\int_0^\infty \frac{k\tilde{p}}{M\omega}\int_0^t \sin[\omega(k)(t-\tau)]\,J_0[k\sqrt{(x-X(\tau))^2+y^2}]\,d\tau\,dk$$
$$-\frac{1}{2\pi}\int_0^\infty \frac{k\tilde{p}}{K}(\cos\omega t)\,J_0(kr)\,dk, \tag{21}$$

where the second term of equation (21) represents the transient effects from removing the static distribution at $t = 0$.

The drag force F_x on the moving load is given by

$$F_x = \int_{-\infty}^\infty\int_{-\infty}^\infty pw_x\,dx\,dy = \frac{1}{4\pi^2}\int_0^\infty\int_0^{2\pi} e^{ikr\cos\alpha X(t)}\,\tilde{p}^*\tilde{w}_x k\,d\alpha\,dk$$
$$= \frac{1}{2\pi}\int_0^\infty\int_0^t \frac{k^2|\tilde{p}|^2}{M\omega}\sin[\omega(t-\tau)]\,J_1[k\{X(t)-X(\tau)\}]\,d\tau\,dk$$
$$+\frac{1}{2\pi}\int_0^\infty \frac{k^2|\tilde{p}|^2}{K}(\cos\omega t)\,J_1[kX(t)]\,dk \tag{22}$$

after the expression in equation (21) is used. Here * indicates complex conjugate.

The time-convolution integrals in equations (21) and (22) can be written more explicitly after a substitution of the translation history defined by equation (2). When this is carried out, the resulting expression will typically consist of three terms, one each for the initial deflection associated with w_0, the acceleration-phase, and the constant-speed phase of the load. In particular, the drag on the moving load can be shown to be of the form

$$F_x(t) = F_x^i(t) + F_x^a(t) + H(t-t_s)F_x^u(t-t_s), \tag{23}$$

where $H(t)$ denotes the Heaviside step function:

$$H(t) = \begin{cases} 0, & t < 0, \\ 1, & t \geq 0. \end{cases}$$

The initial-deflection term $F_x^i(t)$, and the acceleration-phase term $F_x^a(t)$ were recently assessed by Kim & Webster (1988) for a two-dimensional moving pressure problem. As in their case, it was observed that during the accelerating stage, the moving load soon overtook the wave disturbances associated with the initial deflection and the acceleration terms. As a result, surface waves do not accumulate around the loading area, thus contributing minimal effect on the drag. After the constant-speed phase is reached, however, the waves traveling with the same speed as the load accumulate in the load area and contribute significantly to the drag and deflection around the load. The behavior of the constant-speed term $F_x^u(t)$ requires therefore more careful consideration. $F_x^u(t)$ can be evaluated and expressed as follows:

$$F_x^u(t) = \frac{1}{2\pi}\int_0^\infty\int_0^t \frac{k^2|\tilde{p}|^2}{M\omega}(\sin\omega\tau)\,J_1[kU\tau]\,d\tau\,dk, \tag{24}$$

which is the focus of our next discussion.

4. DRAG ON THE MOVING LOAD

The drag component $F_x^u(t)$ could also be interpreted as the force associated with a load starting impulsively from rest at time $t = 0$. Typically, this term approaches an asymptotic (steady) constant value but with oscillations. To understand the behavior of the drag, it suffices to investigate just $F_x^u(t)$ alone as the transient terms in equation (23) eventually decay in time.

4.1. Dispersion Relation

It is helpful to recall the dispersion properties of free waves arising from dispersion relation (19). The celerity $C(k) = \omega/k$ and the group velocity $C_g(k) = \mathrm{d}\omega/\mathrm{d}k$ are given by

$$C(k) = \omega/k = \sqrt{\frac{Dk^4 + \rho g}{mk^2 + \rho k}}, \qquad C_g(k) = \frac{\rho^2 g + Dk^4(4mk + 5\rho)}{2(Dk^5 + \rho g k)^{1/2}(mk + \rho)^{3/2}}, \tag{25}$$

and are shown in Figure 3.

The celerity has a minimum value $C_{\min}$ at $k = k_c$, where

$$\frac{\mathrm{d}C}{\mathrm{d}k} = \frac{Dk^4(2mk + 3\rho) - \rho g(2mk + \rho)}{2k(Dk^5 + \rho g k)^{1/2}(mk + \rho)^{3/2}} = 0 \tag{26}$$

and

$$C(k_c) = C_g(k_c) = C_{\min}, \qquad C''(k_c) = \frac{\omega(k_c)}{k_c}. \tag{27}$$

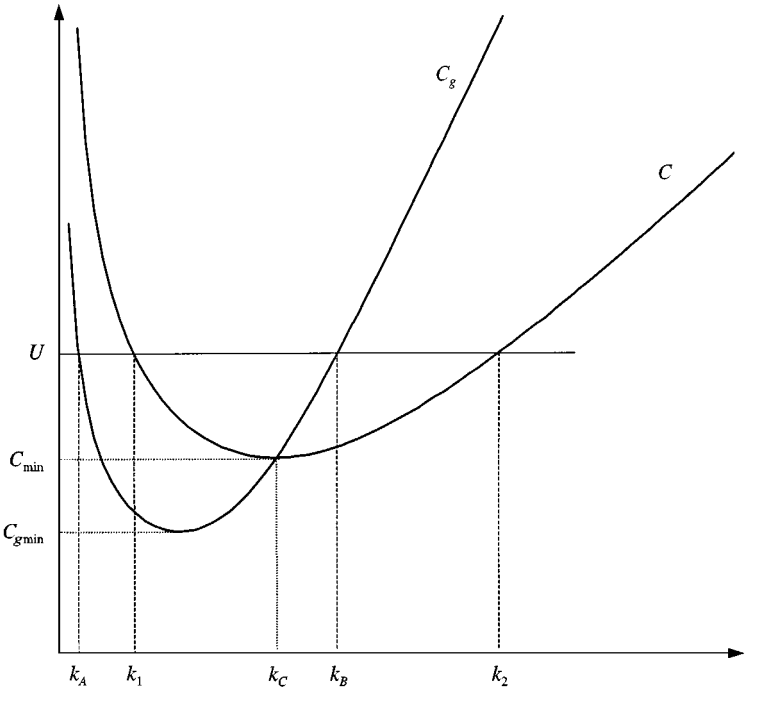

Figure 3. Phase and group velocity of structure–fluid system.

TABLE 1

Some typical dimensions and material properties of floating elastic plates

Case	Ref.	Material	d (m)	D (Nm)	m (kg/m^2)	$C_{\min}$ (m/s)
1	Kashiwagi (1996)	Steel	5·0	$2{\cdot}0\times10^{11}$	$5{\cdot}1\times10^{3}$	33
2	Schulkes & Sneyd (1988)	Ice	2·5	$9{\cdot}8\times10^{9}$	$2{\cdot}3\times10^{3}$	23
3	Yago & Endo (1996)	Steel	2·0	$8{\cdot}0\times10^{9}$	$5{\cdot}1\times10^{2}$	23

The group velocity has also a minimum value $C_{g\min}$, which is less than $C_{\min}$. When $k < k_c$ the wave system has features like gravity waves: the group velocity is less than the celerity and celerity decreases as k increases. When $k > k_c$ the wave system behaves like elastic waves: the group velocity is higher than the celerity, which increases as k increases. As a result, if the load speed U is greater than $C_{\min}$, there are two wave components that can have the same celerity as shown in Figure 3. We denote the wave numbers of the components as k_1 and k_2. These two components are responsible for the transverse waves downstream and upstream of the disturbance, respectively. When $U > C_{g\min}$ the group velocity can match the load speed at $k = k_A$ and k_B, which are wave numbers of wave groups responsible for the asymptotic oscillation in drag, as will be seen later.

The critical speed and corresponding wavelength, for three different configurations of elastic plates, are given in Table 1. In each case, the thickness of the plate is much less than the wavelength ($k_c d \ll 1$), which justifies the thin-plate assumption adopted earlier. Another consequence of this fact is that we can neglect the inertial force due to the mass of the plate since it is much less than the inertial force due to fluid motion.

The ratio between these two inertial forces is $mk_c/\rho = k_c d$, which can be neglected from the thin-plate assumption already introduced. Hereafter, we neglect the mass of the plate without significant loss of the quality of the solution. The effects of mass will also be discussed in connection with the results in Figure 4. Under this assumption, the critical speed and the corresponding wave number can be obtained from equations (25) and (26) as

$$k_c = \left(\frac{\rho g}{3D}\right)^{1/4}, \qquad C_{\min} = 2\left(\frac{g^3 D}{3^3\rho}\right)^{1/8} \simeq 1{\cdot}325\left(\frac{g^3 D}{\rho}\right)^{1/8}, \tag{28}$$

where the " $\simeq$ " sign means "equal within the given significant digits". The minimum group velocity $C_{g\min}$ can be also obtained by differentiating $C_g(k)$ given in equation (25) and setting it equal to zero:

$$C_{g\min} = 0{\cdot}8779\left(\frac{g^3 D}{\rho}\right)^{1/8}. \tag{29}$$

4.2. STEADY-STATE OR LIMITING DRAG

We will first obtain the steady or limiting drag, if it should exist, for the critical condition of $U = C_{\min}$. As $t \to \infty$ the time convolution that appears in equation (24) has the limit

$$\int_0^\infty \sin\omega\tau\ \mathrm{J}_1(kU\tau)\,\mathrm{d}\tau = \begin{cases} \dfrac{C}{Uk\sqrt{U^2 - C^2}}, & U > C, \\ 0, & U < C. \end{cases} \tag{30}$$

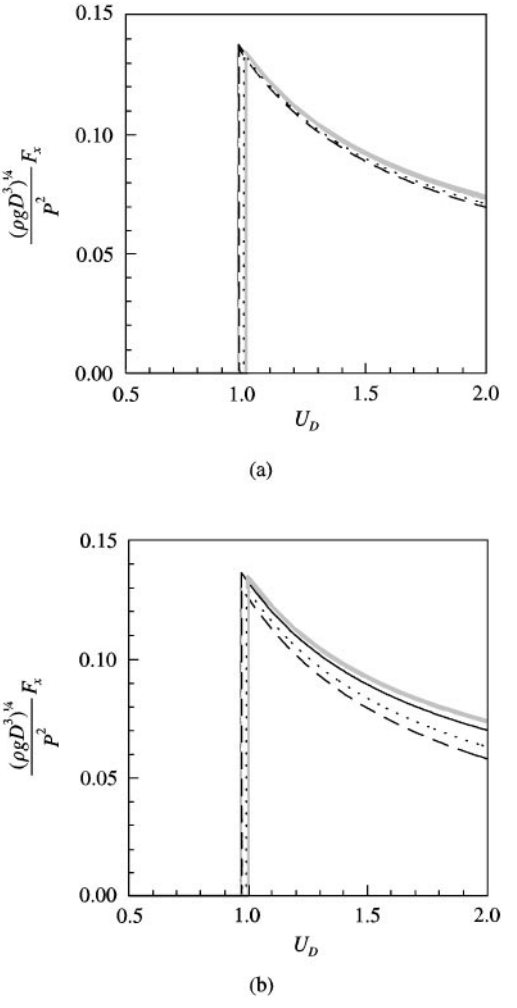

Figure 4. Steady drag of a Gaussian load and a point load: (a) $R = 10$ m; (b) $R = 20$ m. —— Case 1; ----- Case 2 ····· Case 3; ———, point load.

(Gradshteyn & Ryzhik 1965). When $U > C_{\min}$, $C(k) < U$ in the interval $k_1 < k < k_2$. However, when $U < C_{\min}$, $C(k)$ is always greater than U. As a result, we have the steady drag given by

$$F_x^u(\infty) = \begin{cases} 0, & U < C_{\min}, \\ \dfrac{1}{2\pi U} \displaystyle\int_{k_1}^{k_2} \frac{|\tilde{p}|^2}{M\sqrt{U^2 - C^2}}\, \mathrm{d}k, & U > C_{\min}, \end{cases} \tag{31}$$

which has a finite discontinuity at $U = C_{\min}$. The finiteness of the discontinuity can be shown by taking the limit of equation (31) as U approaches $C_{\min}$ from above. To see this, we observe that when k is close to k_c, $C(k)$ can be expanded as

$$C(k) = C_{\min} + \frac{1}{2} C''(k_c)(k - k_c)^2 + \cdots. \tag{32}$$

When U is greater than $C_{\min}$ by a small positive amount δU, k_1 and k_2 can be obtained by evaluating the right-hand side of equation (31) at $C_{\min} + \delta U$:

$$U = C_{\min} + \delta U, \tag{33}$$

$$k_1 = k_c - \delta k, \qquad k_2 = k_c + \delta k, \tag{34}$$

$$\delta k = \left(\frac{2\delta U}{C''(k_c)}\right)^{1/2} = \left(\frac{2k_c \delta U}{\omega''(k_c)}\right)^{1/2}. \tag{35}$$

Using equations (32)–(34), we obtain the limit of the drag when U approaches $C_{\min}$ from above as

$$\begin{aligned} F_c &\equiv \lim_{U \downarrow C_{\min}} F_x^u(\infty) \\ &= \frac{1}{2\pi C_{\min}} \lim_{\delta k \to 0} \int_{-\delta k}^{\delta k} \frac{|\tilde{p}(k_c)|^2}{M(k_c)\sqrt{2C_{\min}}\sqrt{\delta U - \frac{1}{2}C''(k_c)\,k^2}}\,\mathrm{d}k \\ &= \frac{|\tilde{p}(k_c)|^2}{2\pi C_{\min}^{3/2} M\sqrt{C''(k_c)}} \int_{-\delta k}^{\delta k} \frac{1}{\sqrt{\delta k^2 - k2}}\,\mathrm{d}k \\ &= \frac{\sqrt{k_c}\,|\tilde{p}(k_c)|^2}{2C_{\min}^{3/2} M\sqrt{\omega''(k_c)}}. \end{aligned} \tag{36}$$

Since $\omega''(k_c)$ is greater than zero, it confirms that the discontinuity is finite in value. If we substitute equation (28) into equation (36), we have

$$F_c = \frac{0{\cdot}1343|\tilde{p}(k_c)|^2}{(\rho g D^3)^{1/4}}. \tag{37}$$

However, from equation (3) we have $\tilde{p}(k_c) = P\tilde{f}(k_c R)$. Further, we can assume that the radius of the loading is much smaller than the length scale of the deflection, i.e., $k_c R \ll 1$. Under this circumstance, the loading can be treated as a point load of magnitude P, i.e., $\tilde{p}(k_c) \approx P\tilde{f}(0) = P$ and the drag at critical speed given by equation (37) can be expressed rather simply as

$$F_c = \frac{0{\cdot}1343P^2}{(\rho g D^3)^{1/4}}. \tag{38}$$

We note that for point loading, equation (31) can be written as

$$F_x^u(\infty) = \frac{3^{3/8}P^2}{4\pi(\rho g D^3)^{1/4}} \int_{Q(k)>0} \frac{k^{3/2}}{\sqrt{Q(k)}}\,\mathrm{d}k,$$

$$Q(k) = \frac{4}{3^{3/4}}\,U_D^2 k - (k^4 + 1),$$

$$U_D \equiv \frac{U}{C_{\min}} = \frac{3^{3/8}\rho^{1/8}U}{2g^{3/8}D^{1/8}}, \tag{39}$$

which indicates that the steady drag normalized by $P^2/(\rho g D^3)^{1/4}$ can be given as a function of a single parameter, the nondimensionalized speed U_D. Note that $U_D = 1$ when $U = C_{\min}$ and $U_D = 0{\cdot}6627$ when $U = C_{g\,\min}$ from equation (29). The steady drag for point loading is

evaluated using the formula given exactly by equation (39) and plotted in Figure 4. This drag is compared with those obtained using the Gaussian loading given by equation (4), for two different values of R which are chosen unrealistically large, and the three cases given in Table 1. The cases with the Gaussian loading contain the effects of the mass of the plate. It can be seen that the neglect of the mass of the plate and replacement of the distributed loading by a point do not affect the qualitative feature of the phenomenon. The quantitative estimation of the drag by the point-loading formula is quite reasonable except for the Megafloat case where the wavelength on the plate is shorter than for the other cases.

4.3. Asymptotic Transient Behavior of Drag

To evaluate the large-time behavior of equation (24), the method of steepest descent [e.g. Lighthill (1978)] can be used. Using the large-argument representation of the Bessel function, we can deduce the following limiting behavior of the following integral as $t \to \infty$:

$$\int_0^\infty A(k) \sin \omega t \; \mathrm{J}_n\,[kUt]\,\mathrm{d}k$$

$$\sim \sum_{\mathrm{d}\omega/\mathrm{d}k|_{k=k_i}=U} \left[\frac{A(k)}{t\sqrt{k|\omega''|U}} \sin\left\{(\omega - kU)\,t + \frac{n\pi}{2} + (1 + \operatorname{sgn}\omega'')\,\frac{\pi}{4}\right\}\right]_{k=k_i} \tag{40}$$

for any nonsingular bounded function $A(k)$. Note that the stationary points are exactly those designated earlier in Figure 3 as k_A and k_B, with the proviso that U is greater than the minimum group velocity, $C_{g\min}$. If U is less than $C_{g\min}$ these stationary points do not exist on the real k axis and the integral decays exponentially as $t \to \infty$.

Using the above formula (for $n = 1$), we can derive the following asymptotic expression for $F_x^u(t)$:

$$F_x^u(t) = F_x^u(\infty) - \int_t^\infty \frac{\mathrm{d}}{\mathrm{d}t} F_x^u(t)\,\mathrm{d}t$$

$$\sim F_x(\infty) + \frac{1}{2\pi\sqrt{U}} \left[\frac{\sqrt{k_A}|\tilde{p}_A|^2}{M_A C_A \sqrt{|\omega_A''|}}\,\mathrm{Ci}[(\omega_A - k_A U)\,t] \right.$$

$$\left. - \frac{\sqrt{k_B}|\tilde{p}_B|^2 \operatorname{sgn}(\omega_B - k_B U)}{M_B C_B \sqrt{|\omega_B''|}} \left\{ \mathrm{Si}\,[|\omega_B - k_B U|t] - \frac{\pi}{2}\right\}\right], \tag{41}$$

where $M_A \equiv M(k_A)$, $C_A \equiv C(k_A)$, with other variables having subscripts A and B similarly defined. Here, the functions $\mathrm{Ci}(t)$ and $\mathrm{Si}(t)$ are cosine and sine integrals:

$$\mathrm{Ci}(t) = \gamma + \log t + \int_0^t \frac{\cos\tau}{\tau}\,\mathrm{d}\tau,$$

$$\mathrm{Si}(t) = \int_0^t \frac{\sin\tau}{\tau}\,\mathrm{d}\tau, \tag{42}$$

where γ is the Euler constant (Abramowitz & Stegun 1970).

In Figure 5, the time histories of drag, evaluated by numerical integration of equation (24), are plotted for various load speeds. Gaussian quadrature is used for the numerical integration, after deforming the integral path in the complex k-plane to avoid high oscillation of the

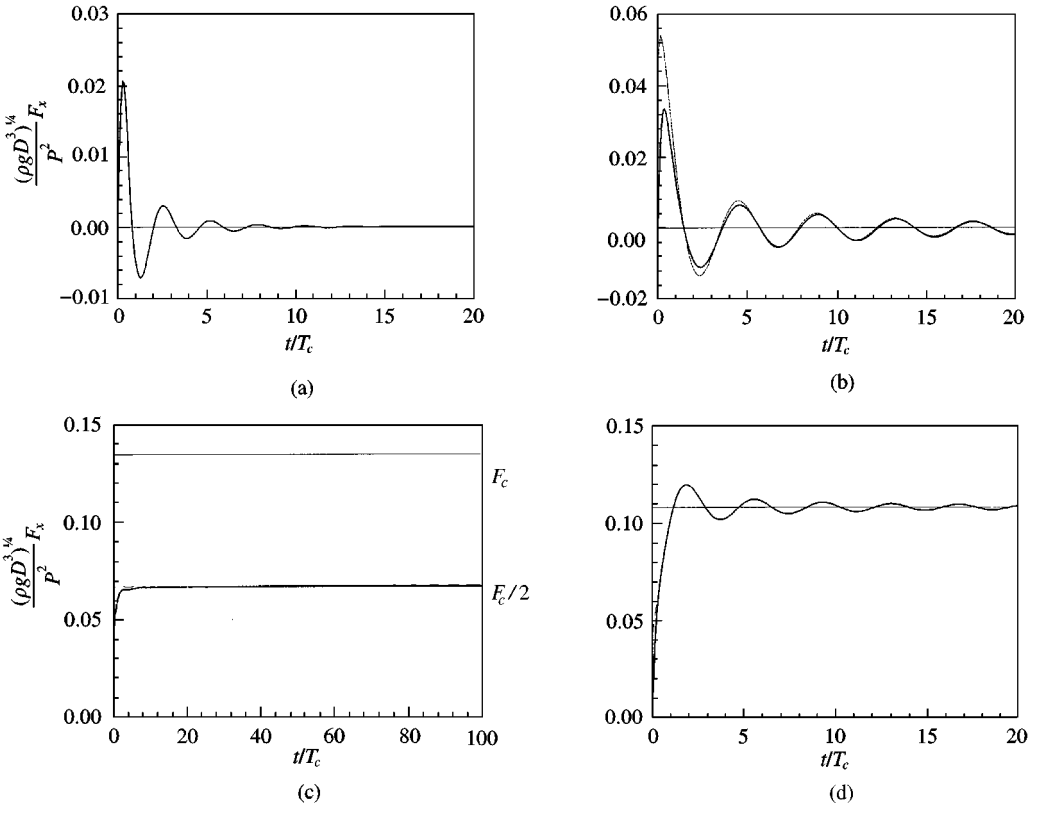

Figure 5. Time history of drag: (a) $U_D = 0{\cdot}0$; (b) $U_D = 0{\cdot}75$; (c) $U_D = 1{\cdot}0$; (d) $U_D = 1{\cdot}25$. Thin straight lines are the limiting steady-state drag; —— numerical integration; ------ asymptotic expansion.

integrand for large time t. When $U > C_{g\min}$, or equivalently $U_D > 0{\cdot}663$, the numerical results are compared with the asymptotic formula given by equation (41). When $U < C_{\min}$ the drag attenuates rapidly after the first peak and approaches zero exponentially with alternating signs. When $U > C_{\min}$ the asymptotic large-t formula compares well with results obtained by numerical integration except, of course, for small t. In these figures, the steady drag as discussed in Section 4.2 is indicated by a thin straight line. The time-dependent drag converges to the steady drag except when $U_D = 1$. The drag converges to $F_c/2$, rather than its steady value F_c. This is the appropriate behavior if one recognizes that the drag experiences a discontinuity at $U_D = 1$ and can be further substantiated by more elaborate limiting analysis.

5. SURFACE DEFLECTION

The foregoing result that the drag is finite for all speed ranges, including at the critical speed, seems to be contradictory to the previous two-dimensional results of Schulkes & Sneyd (1988) which indicated that the deflection and the slope of plate surface increase as $t^{1/2}$ near the loading when $t \to \infty$ for $U = C_{\min}$. Since the drag is proportional to the slope of the deflection near the loading, one would expect that the drag would also increase without bound. This expectation turns out to be not true in our case here.

5.1. Deflection at Load Point at the Critical Speed

For finite values of $\bar{x}$ and y, the growth rate of the deflection of the plate at large t can be obtained by applying the asymptotic formula (40) to the expression of the deflection given by equation (21):

$$\frac{\partial}{\partial t} w^u(\bar{x}, y, t) = -\frac{1}{2\pi} \int_0^\infty \frac{k\tilde{p}}{M\omega} \sin \omega t \, \mathrm{J}_0 [k\sqrt{(\bar{x} + Ut)^2 + y^2}] \, \mathrm{d}k$$

$$\sim -\frac{1}{2\pi\sqrt{Ut}} \left[\frac{\tilde{p}_A}{M_A C_A \sqrt{k_A |\omega_A''|}} \sin \{(\omega_A - k_A U) t - k_A \bar{x}\} \right.$$

$$\left. + \frac{\tilde{p}_B}{M_B C_B \sqrt{k_B |\omega_B''|}} \cos \{(\omega_B - k_B U) t - k_B \bar{x}\} \right] \tag{43}$$

as $t \to \infty$. Note that as in the case of drag, we only need to consider the component related to the constant speed, which will be denoted as w^u in equation (43) and hereafter. The growth rate in equation (43) is asymptotically one-dimensional in $\bar{x}$. This can be explained by the fact that the transient part of the deflection is due to the transverse wave component k_A, which propagates with group speed $C_g = U$, with crest lines normal to the x-axis.

When $U = C_{\min}$, we have $k_B = k_c$ and $\omega_B = \omega_c$ in the second term of equation (43). After performing the necessary time integration, we can obtain:

$$w^u(\bar{x}, y, t) \sim -\frac{\tilde{p}_A}{2\pi M_A C_A \sqrt{k_A U |\omega_A''|}} [(\mathrm{Si}[\psi_A t] - \mathrm{Si}[\psi_A t_0]) \cos k_A \bar{x}$$

$$+ (\mathrm{Ci}[\psi_A t] - \mathrm{Ci}[\psi_A t_0]) \sin k_A \bar{x}]$$

$$- \frac{\tilde{p}_c}{2\pi M_c \sqrt{k_c U^3 |\omega_c''|}} (\cos k_c \bar{x}) \log \frac{t}{t_0} + w^u(\bar{x}, y, t_0) \tag{44}$$

for an arbitrary, finite, reference time t_0. Here $\psi_A \equiv \omega_A - k_A U$. Note that the first term in equation (44) is regular in t, while the second is logarithmic in time, a weaker singular behavior than that of the two-dimensional load. It is of interest to note that the singular term is an even function of $\bar{x}$, thus leading to zero contribution to the drag. This explains why the drag reaches a finite steady-state value, even though the deflection does not tend to steady state. It is worthwhile to note that equation (44) is valid only near the load. More detailed analysis is needed to obtain an expression far away from the load.

To assess the growth of this deflection at the load point for an ice sheet, Schulkes & Sneyd (1988) introduced an amplification factor, which is defined as the ratio of the maximum deflection (Takizawa 1985) or stress (Squire *et al.* 1985) at $U = C_{\min}$ to that at $U = 0$. From our theory, we can develop an estimate of this growth rate by using the asymptotic result of point loading. The deflection at $U = 0$ is the static solution $w_0(x, y)$, which can be obtained from equation (21) by taking $t = 0$. The deflection has a maximum value at $r = 0$:

$$|w_0(0,0)| = \frac{P}{2\pi} \int_0^\infty \frac{k}{Dk^4 + \rho g} \, \mathrm{d}k = \frac{P}{8\sqrt{\rho g D}}. \tag{45}$$

On the other hand, at large time t, we can assume that the maximum deflection for $U = C_{\min}$ is primarily due to the logarithmic term in equation (44). Using equations (25)

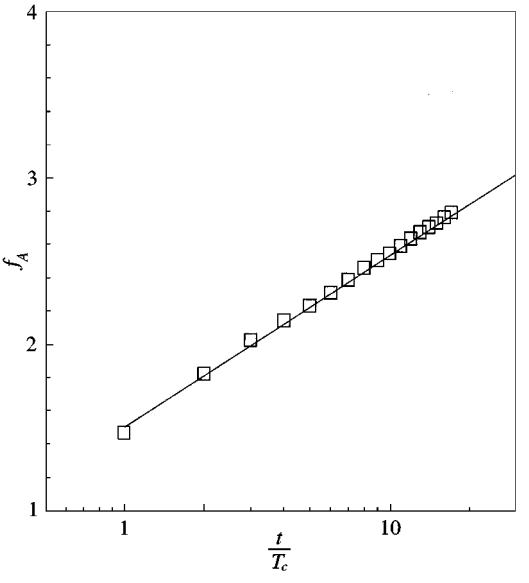

Figure 6. The asymptotic behavior of the amplification factor of surface deflection for $U = C_{\min}$: □ from equation (21); —— $f_A = (\sqrt{2}/\pi) \log t/T_c + 1{\cdot}5$.

and (28), we can express the deflection at $\bar{x} = y = 0$ as

$$w^u(0, 0, t) \sim -\frac{P}{4\pi\sqrt{2\rho g D}} \log t + W, \qquad \text{as } t \to \infty, \tag{46}$$

where W is a constant that can be determined numerically by more precise computations. We have in fact undertaken the numerical evaluation of equation (21) at $\bar{x} = y = 0$ to obtain W. Figure 6 shows the resulting fit of the asymptotic form of the amplification factor $f_A(t)$. Thus, we have managed to extract an equation that describes the growth rate at the critical speed:

$$f_A(t) \equiv \frac{w^u(0, 0, t)}{w_0(0, 0)} \sim \frac{\sqrt{2}}{\pi} \log \frac{t}{T_c} + 1{\cdot}5, \tag{47}$$

where $T_c = \pi(3^5 D/\rho g^5)^{1/8}$ is the period of the wave with minimum celerity.

In the Takizawa (1985) experiment, a vehicle traveled about 100 m at constant speed $C_{\min} = 6$ m/s before reaching the observation point, a travel time of 16·6 s. The flexural rigidity D, estimated from the critical speed and equation (25), is 2×10^5 N m, and we have $f_A = 2{\cdot}3$ from equation (47), compared with the observed value of about 3·0. The agreement is considerably improved compared to the two-dimensional result of Schulkes & Sneyd (1988), which yielded $f_A = 6{\cdot}6$, more than twice the observed value.

5.2. Deflection Surface and Profiles

Encouraged by the good agreement of the foregoing asymptotic results at the critical speed, we computed the deflection pattern for constant speed, $w^u(\bar{x}, y, t)$, which can be obtained from equation (21) with $X(t) = Ut$, for the case of Takizawa's experiment for two values of

U_D. The Fourier integrals were expressed in the Cartesian plane and fast Fourier transforms were used for computing them. In the interest of brevity, we omit the numerical details and only show the perspective views for $U_D = 1{\cdot}5$ and $U_D = 1{\cdot}0$ in Figure 7. The deflection for $U_D = 1{\cdot}5$ and $t/T_c = 4$ can be compared with the experimental result of Takizawa (1985) at $U = 8{\cdot}9$ m/s after the load traveled 100 m. The short wave system in front of the loading is more apparent than the long wave system downstream, as was observed in the experiments. Takizawa reported about four wave crests seen in front of the loading, whereas more than 10 crests are found the computations at larger t. It appears that the upstream short wave system attenuates faster than the model used here because of the viscoelastic properties of ice sheets. At this speed, since $U > C_{\min}$, the deflection reaches a steady state.

When $U_D = 1$, it is seen that the deformation near the loading is growing logarithmically as predicted by equations (46) and (47). The value of $w_{\min}$ is normalized by the maximum static deflection given by equation (45); its decrease (from $-2{\cdot}9$ to $-3{\cdot}5$) is consistent with the logarithmic law: viz. $(\sqrt{2}/\pi)\log(8)$. One also observes, with increasing time, the gradual evolution of the deflection field to a one-dimensional wave system away from the loading as depicted by equation (44) and alluded to earlier in Section 5.1. Note that the growing wave system is symmetric about $\bar{x}$.

To compare with the Takizawa experiment, the behavior of the depression at $y = 1$ m as a function of U_D is shown in Figure 8. The depression was measured when the loading traveled 100 m (or $t = 17$ s). The overall agreement is good. The peak of the experimental results is shifted to a slightly lower speed, which is presumably due to the effect of viscoelastic damping, as postulated by Hosking *et al.* (1988). The undulation of the peak value in our results is due to the transient disturbances which move at a group velocity equal to the speed of the loading. When the loading speed is less than the minimum group velocity, there is no undulation. Near the critical speed, the theoretical result shows slightly lower values than the experiment, as we have seen in the comparison of amplification factor in the previous subsection. The wavelength at the critical speed is 17·5 m, which is slightly longer than the deep water limit for the water depth, $H = 6{\cdot}8$ m. The somewhat less-favorable agreement when ($U > C_{\min}$ may be explained by the effect of finite depth.

5.3. Operations on Floating Runways

First of all, it is comforting to see from the present analysis that when the aircraft transits across the critical speed, it experiences only a bounded drag, even though it may be quite oscillatory in nature. To evaluate the quantitative significance of the resonance phenomenon on realistic floating runways, we estimate the drag, deflection, and slope at the critical speed using formulae (37), (45), and (47) and present them in Table 2. For simplicity, we assume that the loading magnitude $P = 4{\cdot}0 \times 10^6$ N, which is a typical maximum take-off weight of a Boeing-747. To be conservative, weights on all wheels are lumped together. The maximum deflection at the critical speed is obtained by multiplying the amplification factor from equation (47) for running lengths of 4 km. For a given running length, L, the amplification factor can be given as

$$f_A = \frac{\sqrt{2}}{\pi} \log \frac{L}{\lambda_c} + 1{\cdot}5, \tag{48}$$

where $\lambda_c = 2\pi/k_c$ is the wavelength of minimum celerity, which is the assumed to be the critical speed. The maximum slope is obtained by multiplying the wavenumber k_c by the maximum deflection.

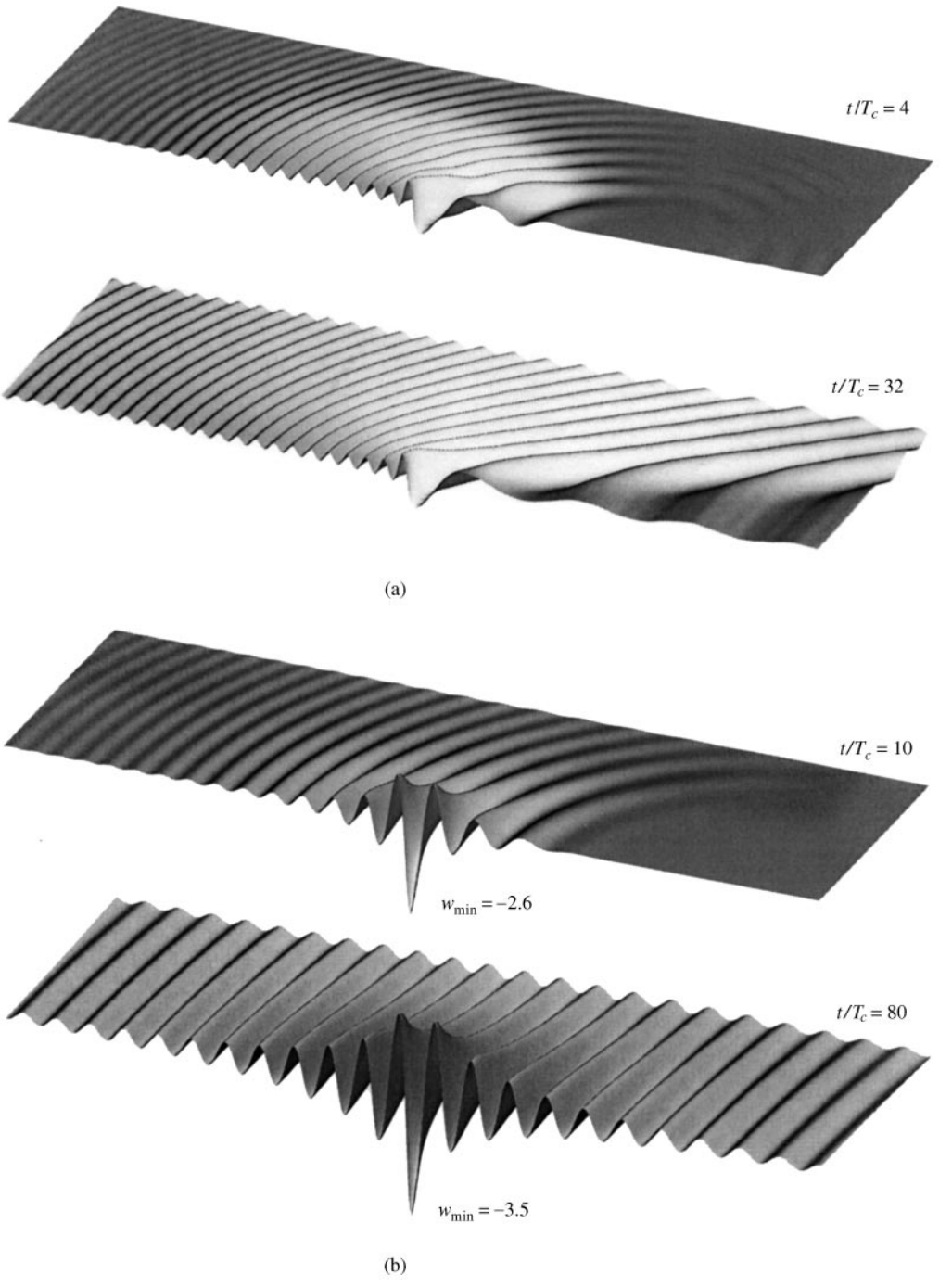

Figure 7. Perspective view of hydroelastic waves generated by impulsively started point load. The deflection is normalized by the maximum static deflection. The plotted area is $-11{\cdot}3 < x/\lambda_c < 11{\cdot}3, 0 < y/\lambda_c < 7{\cdot}6$. The load is moving from right to left, with negative x-values to the right. (a) $U_D = 1{\cdot}5$; (b) $U_D = 1{\cdot}0$.

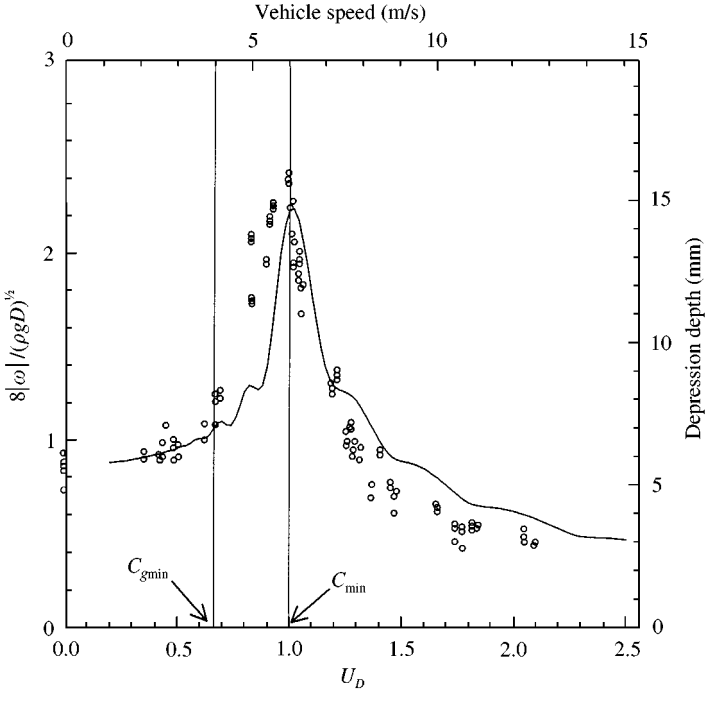

Figure 8. Comparison of predicted depression depth with the Takizawa (1985) experimental results: ——, from present theory for point load, and ○ from experimental results.

TABLE 2

Response at critical speed for $P = 4 \times 10^6$ N

	F_c (N)	$\lvert w_0\rvert_{\max}$ (cm)	$C_{\min}$ (m/s)	f_A^*	$\lvert w^*\rvert_{\max}$ (cm)	Slope* (%)
Case 1	718	1·1	33	2·1	2·7	0·03
Case 2	6910	5·1	23	2·4	14·0	0·33
Case 3	8160	5·6	23	2·4	16·0	0·40

* Evaluated when loading translated 4 km from impulsive start.

For the three cases discussed earlier in Table 1, the steady drag is negligibly small. The drag is about 0·2% of the static weight in the most severe case. The stiffer the structure, the less the drag. Even so, this could constitute as much as 1% of the take-off thrust. The Megafloat model, Case 3, shows a comparatively larger deflection and slope because of its low rigidity, which is expected because it is not a full-scale runway model. For the more realistic runway, Case 1, the deflection is 2·7 cm and the slope is 0·03%, which is not problematic. Thus, for the set of physical properties specified here, the resonant growth of the deflection does not appear to affect the operation of the runway, or at worst, only marginally. However, the conclusion may not be valid if the actual foot-print of the wheels and the finite-width effects of a runway are taken into account.

6. CONCLUSIONS

A three-dimensional analysis of the drag and deflection caused by a translating load on a flexible runway floating on deep water is made within the scope of linear thin-plate and inviscid-fluid theory. Detailed analysis is presented when the load is moving at the critical speed, which is the minimum celerity of the hydroelastic waves of the plate. Contrary to the existing prediction of two-dimensional theory that the drag on a two-dimensional load increases indefinitely in time, we have shown that a steady drag in three dimensions does exist at the critical speed. There is a finite jump at the critical speed, below which there is no steady drag. On the other hand, the deflection around the load at the critical speed grows indefinitely, as $O(\log t)$, which is much weaker than the previously known two-dimensional results of $O(t^{1/2})$. The logarithmic growth rate is found to be in good agreement with some field experiments on ice-sheets.

Based on typical dimensions of runways considered here, the resonant phenomenon at critical speed does not appear to critically affect the take-off operation. Very flexible structures may be the exception. A meager 1% increase in thrust may be needed to overcome this additional structural drag. Other factors such as the foot-print shape of the load and the lateral confinements of the runway may alter the present conclusions.

ACKNOWLEDGEMENTS

The inception of this work was supported by a grant from the Shell Foundation, which the authors gratefully acknowledge. One of us (RWY) is also grateful to the Alexander von Humboldt Foundation for a Humboldt Award at the University of Duisburg where the final stage of the work was completed; and to the Research Institute of Applied Mechanics of Kyushu University for a visit during an earlier stage of the research. This article is SOEST contribution no. 5233 of the University of Hawaii.

REFERENCES

ABRAMOWITZ, M. & STEGUN, A. 1970 *Handbook of Mathematical Functions*, 9th printing. New York: Dover.

DAVYS, J. W., HOSKING, R. H. & SNEYD, A. D. 1985 Waves due to a steadily moving source on a floating ice plate. *Journal of Fluid Mechanics* **158,** 269–287.

ERTEKIN, R. C. & KIM, J. W. 1999 Hydroelastic response of a floating mat-type structure in oblique shallow-water waves. *Journal of Ship Research* **43,** 241–254.

ERTEKIN, R. C., WANG, S. Q. & RIGGS, H. R. 1994 Hydroelastic response of a floating runway. In *Proceedings of the International Conference on Hydroelasticity in Marine Technology*, pp. 389–400, Trondheim, Norway.

GRADSHTEYN, I. S. & RYZHIK, I. M. 1965 *Table of Integrals, Series, and Products*. Orlando: Academic Press.

HOSKING, R. J., SNEYD, A. D. & WAUGH, D. W. 1988 Viscoelastic response of a floating ice plate to a steadily moving load. *Journal of Fluid Mechanics* **196,** 409–430.

KASHIWAGI, M. 1996 A B-spline Galerkin method for computing hydroelastic behavior of a very large floating structure. In *Proceedings of the International Workshop on Very Large Floating Structures, VLFS'96*, pp. 149–156, Hayama, Japan.

KERR, A. D. 1983 The critical velocities of a load moving on a floating ice plate that is subject to in plane forces. *Cold Regions Science and Technology* **6,** 267–274.

KHESHIN, D. Y. 1963 Moving load on an elastic plate which floats on the surface of an ideal fluid (in Russian). *Izvestiia Akademii Nauk SSSR. Otdelenie tekhnicheskikh Mashinostroenie* **1,** 178–180.

KIM, J. W. & WEBSTER, W. C. 1998 The drag of an airplane taking off from a floating runway. *Journal of Marine Science and Technology* **3,** 75–81.

LIGHTHILL, M. J. 1978 *Waves in Fluids*. Cambridge: Cambridge University Press.

MILINAZZO, F., SHINBROT, M. & EVANS, N. W. 1995 A mathematical analysis of the steady response of floating ice to the uniform motion of a rectangular load. *Journal of Fluid Mechanics* **287,** 173–197.

Mamidipudi, M. & Webster, W. C. 1994 The motions performance of a mat-like floating airport. In *Proceedings of International Conference on Hydroelasticity in Marine Technology*, pp. 363–395, Trondheim, Norway.

Nevel, D. E. 1970 Moving loads on a floating ice sheet. U.S. Army CRREL Research Report.

Newman, J. N., Maniar, H. D. & Lee, C.-H. 1996 Analysis of wave effects for very large floating structures. In *Proceedings of the International Workshop on Very Large Floating Structures VLFS'96*, pp. 135–142, Hayama, Japan.

Schulkes, R. M. S. & Sneyd, A. D. 1988 Time-dependent response of floating ice to a steadily moving load. *Journal of Fluid Mechanics* **186,** 25–46.

Squire, V. A., Robinson, W. H., Haskell, T. G. & Moore, S. C. 1985 Dynamic strain response of lake and sea ice to moving loads. *Cold Regions Science and Technology* **11,** 123–139.

Takizawa, T. 1985 Deflection of a floating sea ice sheet induced by a moving load. *Cold Regions Science and Technology* **11,** 171–180.

Yago, K. & Endo, H. 1996 Model experiment and numerical calculation of the hydroelastic behavior of matlike VLFS. In *Proceedings of the International Workshop on Very Large Floating Structures VLFS'96*, pp. 209–216, Hayama, Japan.

Yeung, R. W. 1975, Surface waves due to a maneuvering air-cushion vehicle. *Journal of Ship Research* **19,** 224–242.